nitrogen

MDPI

Article

Structure of Carbon Pools in Surface and Subsurface Horizons of the Main Soil Types in the Russian Arctic

Timur Nizamutdinov [1,*], Vyacheslav Polyakov [1], Anna Shvetsova [1], Egor Artyukhov [1], Anastasia Vainberg [1], Sizhong Yang [2], Xiaodong Wu [2] and Evgeny Abakumov [1]

[1] Department of Applied Ecology, Faculty of Biology, St. Petersburg State University, 7/9 Universitetskaya Nab., St. Petersburg 199034, Russia
[2] Cryosphere Research Station on the Qinghai–Tibet Plateau, State Key Laboratory of Cryospheric Science and Frozen Soil Engineering, Northwest Institute of Eco–Environment and Resources, Chinese Academy of Sciences, 320 Donggang West Road, Lanzhou 730000, China
* Correspondence: t.nizamutdinov@spbu.ru or timur_nizam@mail.ru

Abstract

Arctic and subarctic soils store approximately half of the global soil organic carbon (SOC) pool, yet the structural stability and vulnerability of these carbon reservoirs remain poorly constrained. Most regional assessments treat the cryopedosphere as a homogeneous entity, overlooking the profound taxonomic diversity and vertical stratification that govern carbon stabilization mechanisms. This study investigates the structure of carbon and nitrogen pools across the main soil types of the Russian Arctic (Podzols, Cryosols, Gleysols, and Leptosols) using the soils of the Yamalo-Nenets Autonomous Okrug (YNAO) as an example to elucidate the pedogenic controls on organic matter persistence in permafrost-affected landscapes. Soil profiles were sampled across three geomorphological sites (Lower Ob Basin, Rai-Iz mountain massif, southern Yamal Peninsula). Physical fractionation isolated granulometric fractions with particulate organic carbon (POC), mineral-associated organic carbon (MAOC) and, mineral-associated organic nitrogen (MAON). Topsoil carbon pools exhibited strong taxonomic divergence. Podzols were POC-dominated (86% of SOC) with wide C/N ratios (38), reflecting podzolization and acidic illuviation; Leptosols exhibited the highest MAOC proportion (65%) with narrow C/N ratios (7), indicating rapid mineral stabilization; Cryosols accumulated the highest absolute SOC and total nitrogen (TN) contents but maintained a structurally constrained allocation regardless of total carbon concentration. Subsoil horizons demonstrated shifts toward mineralogical limitation, with near-perfect linear scaling between SOC and MAOC. Vertical decoupling was pronounced, with topsoil SOC poorly predicting subsoil content, and MAOC proportions did not exhibit a statistically significant linear correlation across depths. Carbon stabilization in the Arctic soils is governed by distinct elementary pedogenic processes (podzolization, cryoturbation, gleying, and initial soil formation) operating under divergent climatic constraints. The vertical decoupling of carbon pools and the taxonomic divergence in stabilization mechanisms underscore the need for soil-type-specific parameterization in regional carbon models.

Keywords: soil organic carbon; particulate organic carbon; mineral-associated organic carbon; mineral-associated organic nitrogen; Yamal

Check for updates

Academic Editors: Wenliang Ju, Dengke Ma and Yong Zhang

Received: 14 August 2026
Revised: 29 September 2026
Accepted: 1 October 2026
Published: 5 October 2026

Copyright: © 2026 by the authors. Licensee MDPI, Basel, Switzerland. This article is an open access article distributed under the terms and conditions of the Creative Commons Attribution (CC BY) license.

1. Introduction

Arctic and subarctic ecosystems represent one of the most critical components of the global carbon cycle [1]. Despite covering only a fraction of the Earth's terrestrial surface, high-latitude regions store approximately 50% of the global soil organic carbon (SOC) pool, predominantly locked within permafrost-affected soils and peatlands [2,3]. As global temperatures rise at a rate nearly four times faster in the Arctic than the global average, the stability of these immense carbon reservoirs has become a focal point of contemporary biogeochemical research [4–6]. The potential mobilization of historically sequestered carbon through permafrost thaw, thermokarst formation, and enhanced microbial mineralization—often termed the "permafrost carbon feedback"—poses a significant risk of amplifying anthropogenic climate warming [7,8]. Consequently, accurately quantifying not only the total content but also, more importantly, the structural stability and vulnerability of SOC pools in high-latitude soils is imperative for refining Earth system models and projecting future climate scenarios [9–11].

Modern soil science has increasingly moved beyond the quantification of bulk SOC concentrations toward the physical and chemical fractionation of organic matter into functionally distinct pools [12–15]. The contemporary paradigm recognizes that SOC is not a homogeneous entity but rather a continuum of fractions with vastly different turnover times and stabilization mechanisms [12,13,16]. Specifically, the physical separation of SOC into particulate organic carbon (POC) and mineral-associated organic carbon (MAOC) has emerged as a critical framework for assessing carbon persistence [15,17]. POC, primarily composed of partially decomposed plant debris, is relatively labile and highly susceptible to microbial degradation upon environmental perturbation [18]. In contrast, MAOC consists of low-molecular-weight, microbially derived compounds tightly bound to silt and clay minerals, rendering it highly stable with residence times spanning centuries to millennia [13]. Furthermore, the identification of an inert, chemically recalcitrant SOC fraction (iSOC) is essential for defining the "passive" carbon baseline that is highly resistant to chemical oxidation under current climatic conditions [19,20]. Evaluating the proportional distribution among these fractions (POC, MAOC, and iSOC) is therefore fundamental to distinguishing between vulnerable and protected soil carbon in Arctic landscapes.

Despite the critical importance of these stabilization mechanisms, a significant methodological and conceptual gap persists in the assessment of Arctic carbon pools. The vast majority of regional studies have historically treated the Arctic cryopedosphere as a relatively uniform entity, predominantly focusing on bulk SOC accumulation in peat-forming Histosols or the upper cryoturbated horizons of Cryosols [21,22]. This "bulk-centric" approach frequently overlooks the profound taxonomic diversity of subarctic landscapes, where Podzols, Gleysols, and Leptosols coexist and drive divergent biogeochemical pathways [2,23]. Moreover, the existing literature heavily biases sampling efforts toward surface horizons (topsoil), largely neglecting the vertical stratification and stabilization dynamics occurring in subsurface horizons and near the permafrost table [15,24]. Recent evidence suggests that subsurface soils operate under fundamentally different biogeochemical constraints, where carbon stabilization is often strictly limited by mineral sorption capacity rather than by biogenic input rates [25–27]. Failing to account for this taxonomic and vertical heterogeneity leads to systematic errors in regional carbon inventories, potentially misclassifying highly stable, mineral-protected deep carbon as vulnerable, or conversely, underestimating the lability of surface particulate accumulations.

To address these critical knowledge gaps, this study investigates the structural distribution of carbon and nitrogen pools across the main soil types of the Yamalo-Nenets Autonomous Okrug (YNAO), a key region of the Russian Arctic experiencing rapid climatic and anthropogenic transformation [28].

By employing rigorous physical and chemical fractionation protocols to isolate POC, MAOC, and iSOC fractions, combined with comprehensive stoichiometric and regression analyses across both surface and subsurface horizons, we aim to:

(1) Quantify the absolute concentrations and proportional contributions of labile, stabilized, and inert carbon and nitrigen pools across Podzols, Cryosols, Gleysols, and Leptosols;
(2) Evaluate the vertical decoupling and horizon-specific stabilization mechanisms governing carbon persistence;
(3) Elucidate the pedogenic controls ranging from elementary pedogenic processes that dictate the partitioning of organic matter in subarctic ecosystems.

2. Materials and Methods

2.1. Study Area and Environmental Conditions

The research was conducted in the Yamalo-Nenets Autonomous Okrug (Russian Federation) across three distinct bioclimatic and geomorphological zones: the Lower Ob Basin, the Rai-Iz mountain massif (Polar Urals), and the southern Yamal Peninsula (Figure 1). Climatic conditions correspond to the subarctic type (Dfc according to the Köppen classification).

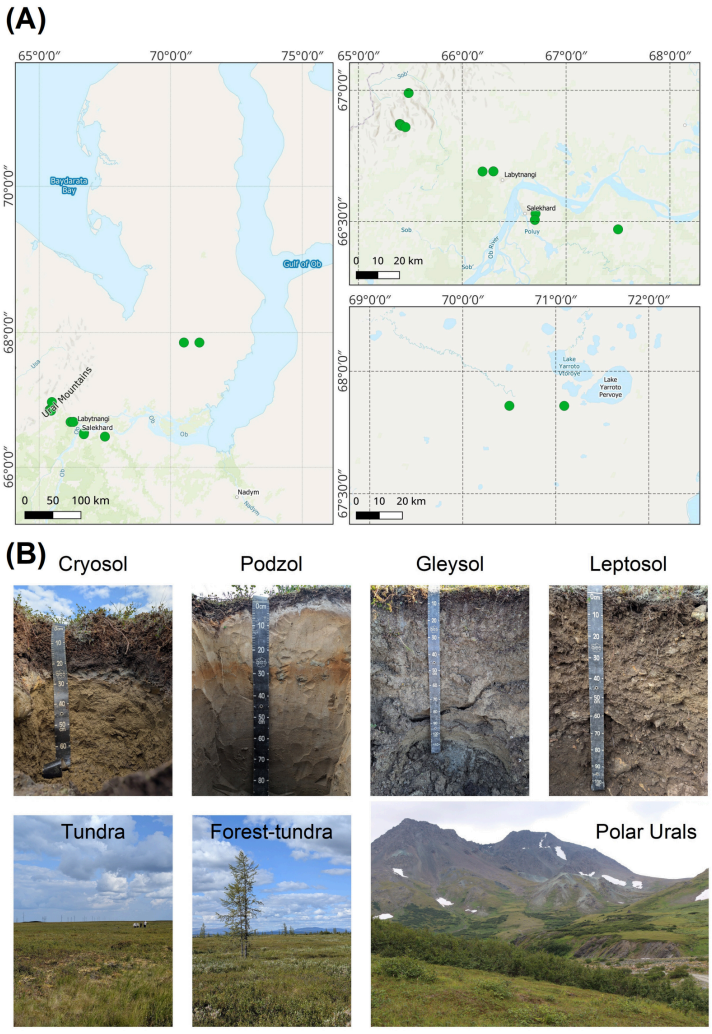


Figure 1. (**A**) Location of sampling sites (green circles) in Yamalo-Nenets Autonomous Okrug. (**B**) Typical profiles for each studied soil type and landscapes of Yamalo-Nenets Autonomous Okrug.

The first study area is situated in the northern part of the Lower Ob Basin, adjacent to the cities of Salekhard and Labytnangi. The regional climate is characterized by a mean annual air temperature (MAT) of −5.1 °C and mean annual precipitation (MAP) of approximately 500 mm. Parent materials consist of polygenetic and polydisperse Neopleistocene–Holocene sedimentary deposits. The dominant vegetation includes dwarf shrubs (*Betula nana*, *Vaccinium uliginosum*, *Andromeda polifolia*), willow shrubs (*Salix* spp.), and lichens (*Cladonia* and *Cetraria* spp.). Within this region, two key sites were established: a polygonal forest-tundra plain southwest of Salekhard, where Albic Podzols are formed; and a micro-elevated wetland in the foothill forest-tundra near Labytnangi, characterized by Histic Cryosols developed on medium-loamy boulder and pebbly deposits. These Cryosols exhibit thixotropic properties and a distinct tangled-layered structure rather than defined structural aggregates.

The second research site is located in the Rai-Iz mountain massif of the Polar Urals. This alpine environment experiences harsher climatic conditions, with a MAT of −8.2 °C and MAP ranging from 700 to 1000 mm. The ground cover is predominantly composed of lichens, dwarf shrubs (*B. nana*, *A. polifolia*), and specialized alpine flora such as *Dryas octopetala*, *Salix polaris*, *S. arctica*, *Silene acaulis*, *Dianthus repens*, and *Saxifraga spinulosa* growing among bedrock outcrops. Two key sites were sampled: (i) a gentle slope featuring Skeletic and Histic Cryosols with a high proportion of gravel and large angular rock fragments; and (ii) a steeper slope with accumulated colluvial deposits, where Skeletic Leptosols with an undifferentiated soil profile have developed. The fine earth of the Leptosols is dark brown, permeated by plant roots to a depth of 40 cm, and the profile exhibits 70–80% stoniness dominated by large, angular bedrock blocks.

The third study site was located in the southern part of the Yamal Peninsula. The climate here is harsher, with a MAT of −10 °C and a MAP ranging from 230 to 270 mm. The projective vegetation cover is predominantly composed of lichens (*Cladonia* sp., *Cetraria* sp.) and dwarf shrubs (*Vaccinium uliginosum*, *Empetrum nigrum*, and *Betula nana*). The soils in this region form on layered sandy gleyed deposits. The first key plot was located in the southern hypoarctic tundra subzone, near lakes Ngevadyodato and Yakhadymalto, where Turbic Podzols are developing. The second key plot was established adjacent to the Yaroto lakes, where Entic Podzols are forming.

In addition to the aforementioned soils, Gleysols were sampled to represent poorly drained, hydromorphic landscapes within the study region. These soils were primarily located in thermokarst depressions and flat lowlands characterized by prolonged surface waterlogging and restricted internal drainage. The parent materials predominantly consist of heavy loamy deposits. Due to the persistent anaerobic conditions, these profiles exhibited pronounced gleyic properties and were classified as Histic or Folic Gleysols.

In total, 36 soil profiles were sampled across three geomorphological sites: 6 Podzols, 6 Leptosols, 18 Cryosols, and 6 Gleysols. Detailed coordinates and site descriptions are provided in Table A1 in Appendix A.

Soil classification was performed following the World Reference Base for Soil Resources (4th edition) system [29].

2.2. Soil Sampling and Sample Preparation

Field campaigns were executed in August 2024. At each study site, representative soil profiles were dug to characterize the morphological properties of the soils. Soil samples were collected at fixed depth intervals (0–15 cm for topsoil and 15–30 cm for subsoil) to ensure cross-taxa comparability and alignment with standard modeling depths. These intervals do not correspond to single genetic horizons; the material captured within each interval varied by taxon. Podzols—0–15 cm: O/AE; 15–30 cm: Bs/C. Cryosols—0–15 cm:

Ah; 15–30 cm: Bw/C and permafrost-affected C. Gleysols—0–15 cm: A/Bg; 15–30 cm: Bg/C. Leptosols—both intervals: undifferentiated A/C horizon.

To account for micro-spatial heterogeneity, three subsamples were collected from different vertical walls of each soil pit using a clean steel shovel per depth interval.

Immediately following extraction, the soil samples were air-dried on-site under ambient field conditions to halt microbial activity and prevent the degradation of labile organic fractions during transit. The pre-dried samples were then homogenized, placed in sterile, sealed plastic bags, and transported to the laboratory facilities in St. Petersburg for subsequent physical, chemical, and structural analyses of the carbon and nitrogen pools.

2.3. Laboratory Analysis and Physical Fractionation

Prior to the preparation of the composite samples, all field-moist subsamples were air-dried at room temperature (24–25 °C) to constant weight and passed through a 2 mm sieve to remove coarse roots, stones, and large organic debris. A composite sample (approximately 800–1000 g) was subsequently prepared by thoroughly mixing equal mass proportions of the three pre-sieved subsamples.

Determination of soil pH was carried out in soil–water (soil-to-water ratio 1:2.5 w/v) solution [30]. Particle-size distribution (clay (<0.001 mm) and silt (<0.01 mm)) were measured by pipette method without preliminary removal of soil organic matter but with dispersion of the sample with a 4% $Na_4P_2O_7$ solution. It should be noted that the clay fraction was defined as <0.001 mm (1 μm) following the Russian national soil classification system [31], which distinguishes fine clay as a separate fraction.

Physical fractionation followed Muratore & Welsh [32]: 5 g of soil was dispersed in 0.5% sodium hexametaphosphate, agitated for 24 h, and wet-sieved at 53 μm. The >53 μm fraction (POC-containing) and the <53 μm fraction (MAOC/MAON-containing) were dried, weighed (mass recovery 95–100%), and analyzed for C and N.

The chemical inert SOC (iSOC) fraction was isolated by sequential oxidation with 30% H_2O_2 at 80–90 °C until effervescence ceased [33].

In the bulk soil, chemical-oxidized soil and dried fine fractions (<53 μm), the concentration of organic carbon was determined using the Walkley–Black method (with correction factor 1.3), utilizing the colorimetric modification outlined by the Food and Agriculture Organization of the United Nations (FAO) [34]. Total nitrogen (TN) content in the same fractions was measured via the Kjeldahl method, following the FAO titrimetric modification [35].

2.4. Statistics and Calculations

To elucidate the internal architecture, stoichiometric coupling, and scaling relationships between the different organic carbon pools, linear regression analyses were conducted. Bivariate relationships (e.g., total SOC vs. absolute MAOC, bulk C/N vs. C/N in fine fraction) were evaluated by calculating Pearson's correlation coefficient (r) and the coefficient of determination (R^2). To decouple overarching landscape trends from soil-specific biogeochemical mechanisms, these regression models were fitted both to the pooled dataset and individually for each soil taxon, stratified by horizon depth (topsoil vs. subsoil). For all statistical tests, a probability level of $p < 0.05$ was considered to indicate statistical significance. Adjusted p-values resulting from the post hoc corrections are explicitly reported in Section 3 to ensure full transparency regarding the significance of pairwise differences. All statistical analyses, data visualization, and mathematical modeling were performed using standard scientific computing environments (Origin(Pro), Version 2024. OriginLab Corporation, Northampton, MA, USA).

Detailed calculation procedures (Equations (A1)–(A6)) and the full statistical workflow are provided in the Appendix B.

3. Results

3.1. General Physicochemical and Textural Properties

Prior to the physical fractionation of organic matter pools, the baseline physicochemical and textural properties of the soil profiles were characterized to establish the mineralogical and environmental context for carbon stabilization mechanisms. Soil reaction exhibited a stark dichotomy driven by soil taxonomy and dominant pedogenic processes. Podzols and peat-forming profiles were characterized by strongly to very strongly acidic conditions, with pH 4.2 ± 0.2. In contrast, Leptosols developing on richer parent materials or in cryoturbated landscapes displayed moderately acidic to neutral reactions, with pH values 6.6 ± 0.3, reflecting a higher base saturation and limited leaching (Table 1).

Table 1. General properties of studied soils for topsoil and subsoil layers.

Soil	N	SOC	MAOC	TN	MAON	iSOC	C/N	pH	Clay
	Pits	g kg^{-1}							%
Topsoil									
Podzol	6	215 ± 37	30.1 ± 7.0	6.5 ± 0.8	1.9 ± 0.6	35.4 ± 11.1	38.5 ± 5.3	4.2 ± 0.2	2.5 ± 1.9
Leptosol	6	14.2 ± 3.7	9.0 ± 1.6	2.6 ± 1.0	0.9 ± 0.3	3.4 ± 2.6	6.9 ± 2.1	6.6 ± 0.3	8.0 ± 2.7
Cryosol	18	161 ± 59	32.5 ± 14.4	10.4 ± 4.6	2.3 ± 0.5	25.7 ± 15.8	20.6 ± 7.4	4.3 ± 0.1	24.6 ± 4.5
Gleysol	6	45.2 ± 23.5	13.4 ± 6.4	4.9 ± 3.5	1.8 ± 1.1	2.31 ± 1.42	12.8 ± 4.9	4.4 ± 0.1	14.1 ± 6.5
Subsoil									
Podzol	6	12.9 ± 7.6	5.76 ± 3.91	-	-	-	-	4.4 ± 0.1	3.1 ± 1.2
Leptosol	6	19.9 ± 12.1	11.3 ± 6.3	-	-	-	-	7.1 ± 0.1	10.9 ± 2.0
Cryosol	18	18.9 ± 21.8	12.2 ± 13.1	-	-	-	-	5.2 ± 0.2	27.8 ± 2.7
Gleysol	6	14.5 ± 7.9	7.56 ± 3.91	-	-	-	-	4.5 ± 0.1	14.4 ± 6.2

Particle-size distribution analysis further highlighted a textural divergence across the studied landscapes. Podzol profiles were predominantly sandy and loamy sands, heavily dominated by the fine sand fraction (0.25–0.05 mm), which frequently accounted for 70% to over 90% of the mineral matrix, with minimal contributions from silt and clay fractions. Conversely, the Cryosols and Leptosols exhibited highly heterogeneous, polydisperse textures ranging from sandy loams to silt loams and silty clays. These profiles were characterized by substantial accumulations of coarse silt (0.05–0.01 mm, reaching up to 42%) and clay fractions (<0.001 mm, up to 30%).

3.2. Absolute Concentrations of Carbon Pools in Surface Horizons

The quantitative assessment of SOC and its physical fractions in the surface horizons (topsoil) of the Yamalo-Nenets Autonomous Okrug revealed substantial heterogeneity across the main soil types (Figure 2). The total SOC content varied widely, ranging from marginal accumulations in Leptosols (14.2 ± 3.7 g kg^{-1}) to massive content in Podzols (215 ± 37 g kg^{-1}). Cryosols also exhibited high, albeit highly variable, SOC concentrations (161 ± 59 g kg^{-1}), while Gleysols demonstrated intermediate values (45.2 ± 23.5 g kg^{-1}).

A one-way analysis of variance (ANOVA) confirmed a highly significant effect of soil genesis on the absolute SOC concentrations ($p < 0.001$). Subsequent pairwise comparisons utilizing the Dunn-Sidak correction highlighted distinct biogeochemical groupings. Podzols accumulated significantly more total SOC than both Gleysols ($p < 0.001$) and Leptosols ($p < 0.001$). Similarly, Cryosols exhibited significantly higher SOC concentrations compared

to Gleysols ($p < 0.001$) and Leptosols ($p < 0.001$). Interestingly, the difference between the two most carbon-rich soil types (Podzols and Cryosols) was not statistically significant.

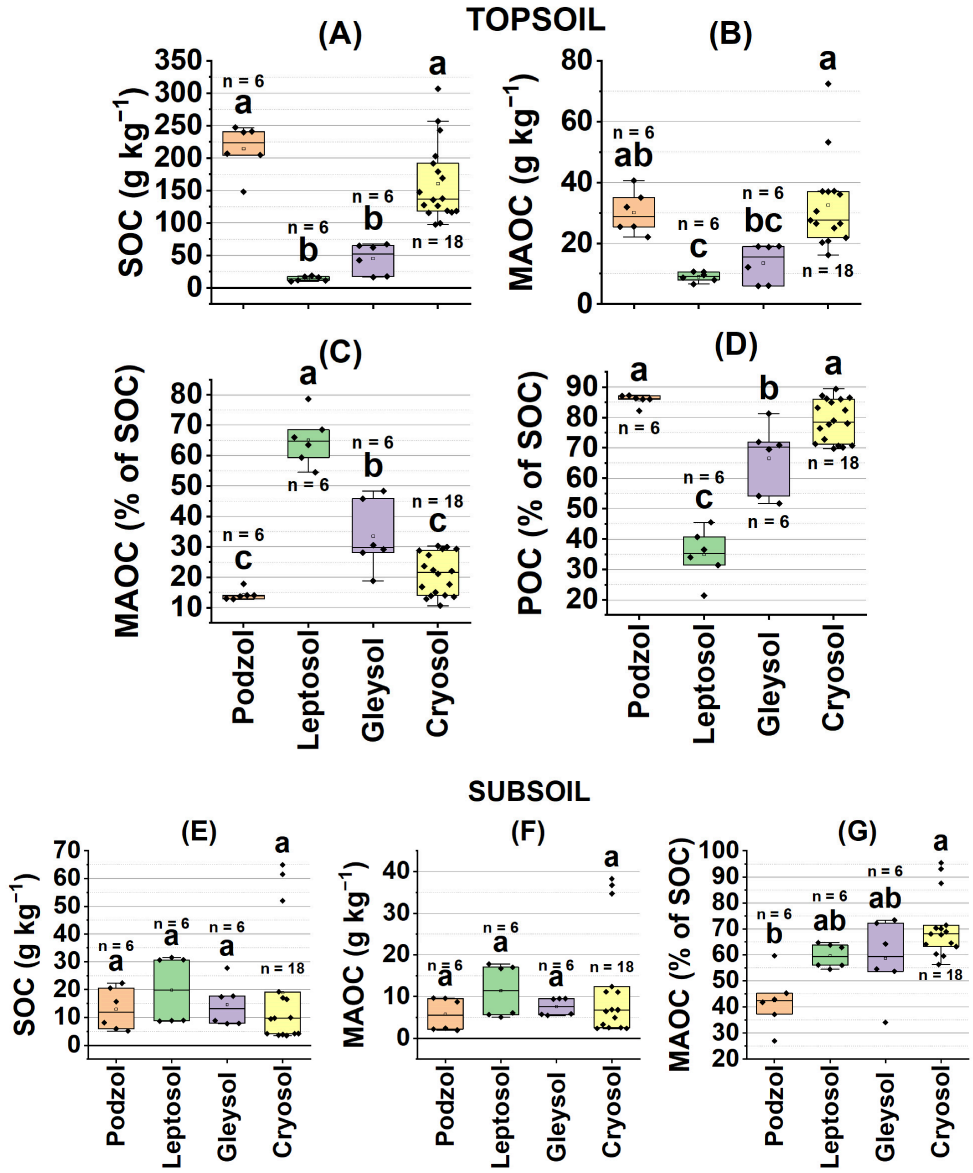


Figure 2. Box plots of measured parameters across soil types in **topsoil** and **subsoil** horizons. (**A**) Soil organic carbon (SOC) content (g kg^{-1}) in topsoil. (**B**) Mineral-associated organic carbon (MAOC) content (g kg^{-1}) in topsoil. (**C**) MAOC proportion (% of SOC) in topsoil. (**D**) Particulate organic carbon (POC) proportion (% of SOC) in topsoil. (**E**) SOC content (g kg^{-1}) in subsoil. (**F**) MAOC content (g kg^{-1}) in subsoil. (**G**) MAOC proportion (% of SOC) in subsoil. Whiskers indicate standard deviations. The exact sample size (*n*) and post hoc significance (lowercase letters) are printed directly on each panel.

This divergence was mirrored in the absolute concentrations of the iSOC and MAOC fractions (Figures 2B,C and A1 (Appendix C)). The ANOVA revealed significant variations in both iSOC ($p < 0.001$) and MAOC ($p < 0.001$). The Dunn–Sidak test demonstrated that Podzols possessed significantly higher absolute amounts of iSOC (35.4 ± 11.1 g kg^{-1}), representing the accumulation of highly stable, decomposition-resistant organic matter, compared to all other soil types ($p < 0.01$ for all pairwise comparisons). In contrast, Leptosols were characterized by the lowest MAOC concentrations (9.0 ± 1.6 g kg^{-1}), which were significantly lower than those in Podzols ($p < 0.001$) and Cryosols ($p < 0.01$).

3.3. Structural Distribution and Stabilization of Carbon Pools

While absolute carbon concentrations reflect the overall bioclimatic accumulation potential, the relative structural distribution of SOC fractions (expressed as percentages of total SOC) provides critical insights into the mechanisms of carbon stabilization. The ANOVA indicated a profound effect of soil type on the proportional distribution of POC and MAOC ($p < 0.001$ for both fractions, as they sum to 100%).

Podzols exhibited a strongly POC-dominated surface horizon (Figure 2C,D) structure, with an average of 85.8 ± 1.9% of the total SOC. This structural dominance of POC in Podzols was significantly higher than in Gleysols (66.5 ± 11.4%, $p < 0.05$), Leptosols (34.9 ± 8.3%, $p < 0.001$), and Cryosols (79.0 ± 6.9%, $p < 0.001$). Conversely, Leptosols demonstrated a different stabilization paradigm, with the MAOC fraction accounting for the majority of the surface SOC (65.1 ± 8.3%). Gleysols and Cryosols occupied an intermediate structural position: Gleysols had a significantly higher MAOC proportion (33.4 ± 11.4%) compared to Cryosols (21.0 ± 6.9%, $p < 0.05$).

The relative proportion of the iSOC in SOC pool (Appendix C, Figure A1) did not exhibit a statistically significant main effect across the studied soil types at the conventional α level ($p = 0.057$). However, the post hoc Dunn–Sidak test identified a specific significant divergence between Podzols and Gleysols ($p < 0.001$).

3.4. Absolute Carbon Contents and Divergent Stabilization in Subsurface Horizons

Unlike the pronounced divergence observed in the surface horizons, the structural dynamics of carbon pools in the subsurface horizons (subsoil) exhibited a marked convergence in absolute concentrations across the studied soils (Figure 2E–G). A one-way ANOVA revealed no significant main effect of soil type on the absolute concentrations of either total SOC ($p = 0.83$) or the MAOC fraction ($p = 0.50$). Mean SOC values in the subsoil ranged from 12.9 ± 7.6 g kg^{-1} in Podzols to 19.9 ± 12.1 g kg^{-1} in Leptosols, with Cryosols demonstrating a high degree of spatial heterogeneity (18.9 ± 21.8 g kg^{-1}). Consequently, the post hoc test confirmed the absence of statistically significant pairwise differences in absolute carbon contents between any of the soil types in the subsoil ($p > 0.05$ for all comparisons).

The proportion of MAOC relative to total SOC in the subsoil varied significantly among soil types ($p < 0.001$). Subsurface horizons of Cryosols were overwhelmingly dominated by the mineral-associated fraction, with MAOC accounting for an average of 70.7 ± 11.9% of the total SOC pool. The proportional dominance in Cryosols was significantly higher than that observed in the subsoils of both Podzols (42.3 ± 10.7%, $p = 0.002$) and Leptosols (59.6 ± 4.6%, $p < 0.05$). Gleysols (58.6 ± 14.7%) occupied an intermediate structural position, showing no significant divergence, but maintaining a notably higher MAOC proportion than the Podzols.

3.5. Nitrogen Pools and Structural Partitioning in Surface Horizons

To further elucidate the biogeochemical mechanisms driving carbon stabilization, the distribution of TN and its mineral-associated fraction (MAON) was evaluated in the topsoil (Figure 3). The nitrogen dynamics exhibited a strong dependence on soil taxonomy, mirroring the broad accumulation patterns observed for carbon. ANOVA revealed highly significant differences in absolute TN concentrations among the soil types ($p < 0.001$). Cryosols accumulated the highest TN content (10.4 ± 4.6 g kg^{-1}), which were significantly greater than those in both Leptosols (2.6 ± 1.0 g kg^{-1}, $p < 0.001$) and Podzols (6.5 ± 0.8 g kg^{-1}, $p = 0.035$). Podzols also contained significantly more TN than the severely depleted Leptosols ($p < 0.001$). Gleysols displayed intermediate TN concentrations (4.9 ± 3.5 g kg^{-1}), showing a marginal, albeit non-significant, trend of being lower than Cryosols ($p = 0.07$).

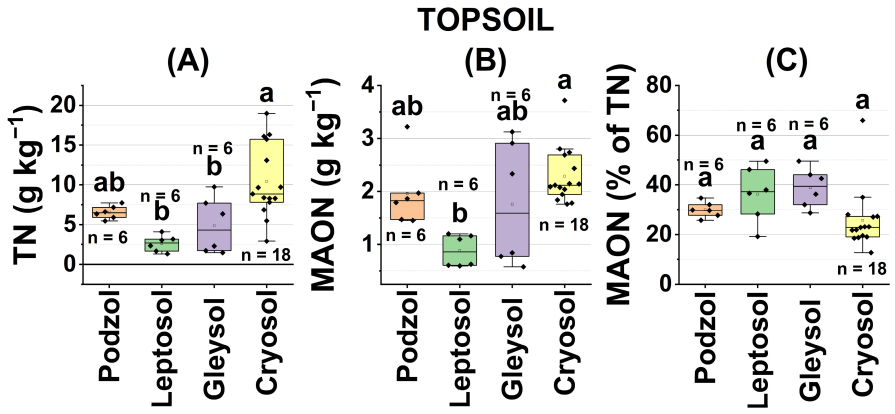


Figure 3. Box plots of measured parameters across soil types in **topsoil** horizons. (**A**) Total nitrogen (TN) content (g kg^{-1}). (**B**) Mineral-associated organic nitrogen (MAON) content (g kg^{-1}). (**C**) MAON proportion (% of TN). Whiskers indicate standard deviations. The exact sample size (*n*) and post hoc significance (lowercase letters) are printed directly on each panel.

This hierarchy of absolute accumulation was largely preserved in the MAON pool ($p = 0.002$). Cryosols (2.3 ± 0.5 g kg^{-1}) and Podzols (1.9 ± 0.6 g kg^{-1}) harbored significantly more mineral-associated nitrogen than Leptosols (0.9 ± 0.3 g kg^{-1}, $p < 0.001$ and $p = 0.046$, respectively). However, when evaluating the structural partitioning of nitrogen, the relative proportion of MAON to total TN (ranging from 25.6% to 38.8%) showed only a marginal main effect of soil type ($p = 0.046$), with no statistically significant pairwise differences.

3.6. Stoichiometric Signatures in Bulk Soil and in Fine Fraction

The stoichiometric signatures of the soil organic matter (C/N ratios) provided profound insights into the decomposition pathways and the biochemical quality of the stabilized organic matter (Figure 4). The bulk soil C/N ratio exhibited the most pronounced divergence among the studied soils ($p < 0.001$). Podzols were characterized by wide C/N ratios (38.5 ± 5.3). The Dunn–Sidak test confirmed that the C/N ratio in Podzols was significantly wider than in Cryosols (20.6 ± 7.4, $p < 0.001$), Gleysols (12.8 ± 4.9, $p < 0.001$), and Leptosols (6.9 ± 2.1, $p < 0.001$). Cryosols also exhibited significantly wider bulk C/N ratios compared to Leptosols ($p < 0.001$).

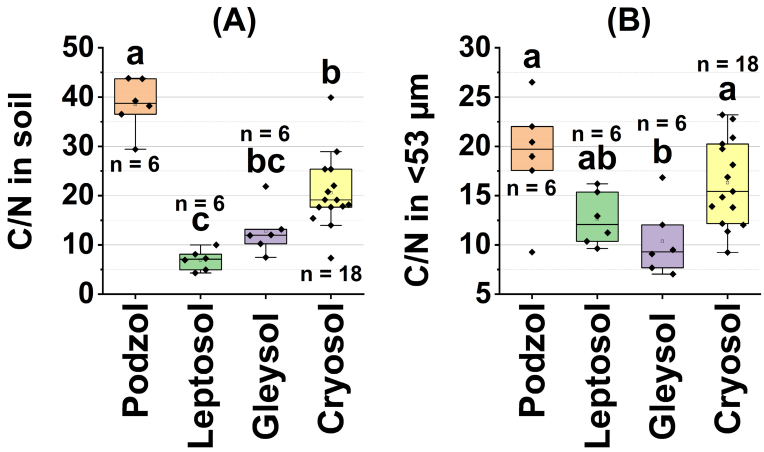


Figure 4. Box plots of measured parameters across soil types in **topsoil** horizons. (**A**) C/N ratio in bulk topsoil samples of topsoil. (**B**) C/N ratio in <53 µm fraction of topsoil. Whiskers indicate standard deviations. The exact sample size (*n*) and post hoc significance (lowercase letters) are printed directly on each panel.

Crucially, the stabilization of organic matter onto fine mineral surfaces resulted in a universal narrowing of the C/N ratio within the fine (<53 µm) fraction compared to the bulk soil (Figure 4B). Nevertheless, significant inter-type variations persisted in the fine fraction stoichiometry ($p = 0.005$). The C/N ratio in the fine fraction of Gleysols was the narrowest (10.4 ± 3.6), which was significantly lower than that of Cryosols (16.3 ± 4.4, $p = 0.048$). Notably, Podzols maintained a relatively wide C/N ratio even within the <53 µm fraction (19.1 ± 5.7).

3.7. Bivariate Relationships

To further elucidate the internal architecture of the soil organic matter and the scaling relationships between different carbon and nitrogen pools, linear regression analyses were performed across the entire dataset (Figure 5). In the surface horizons, strong positive scaling relationships were observed among the absolute pools. Total SOC was a robust predictor (Figure 5A) of absolute MAOC ($R^2 = 0.65$, r = 0.80) and iSOC ($R^2 = 0.53$, r = 0.73) (Figure 5B). Similarly, a strong stoichiometric coupling was identified between the mineral-associated fractions, with MAOC significantly predicting (Figure 5I) MAON concentrations ($R^2 = 0.51$, r = 0.714).

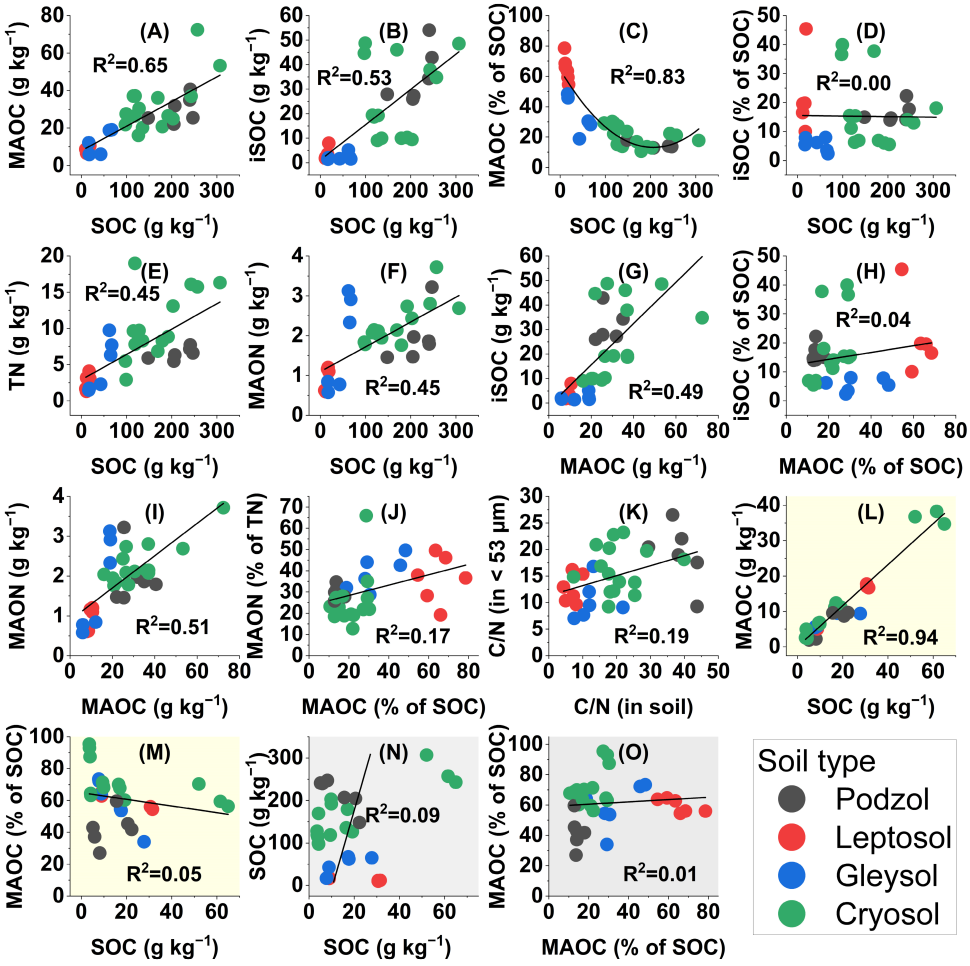


Figure 5. Bivariate relationships ($n = 36$) between measured parameters. (**A**–**J**) Topsoil horizons. (**K**) Relationship of C/N ratio in bulk soil and <53 µm fraction in topsoil. (**L**,**M**) Subsoil horizons. (**N**) Relationship of soil organic carbon (SOC) content in topsoil and subsoil. (**O**) Relationship of mineral-associated organic carbon (MAOC, % of SOC) in topsoil and subsoil.

In contrast, the relative structural distribution of these pools exhibited divergent scaling behaviors. While the proportion of MAOC relative to total SOC (Figure 5C) showed

a strong relationship with total SOC (R^2 = 0.83), the relative proportion of iSOC was entirely independent (Figure 5D) of the total SOC concentration (R^2 = 0.00, r = −0.02). Furthermore, the proportional allocations into MAOC and iSOC (Figure 5H) were not correlated with each other (R^2 = 0.04, r = 0.19).

The stoichiometric relationships further highlighted the decoupling of bulk and stabilized fractions. While absolute SOC and TN (Figure 5E) were moderately coupled (R^2 = 0.45, r = 0.67), the relationship between their respective stabilization proportions (MAOC % of SOC vs. MAON % of TN) was considerably (Figure 5J) weaker (R^2 = 0.17, r = 0.42). Crucially, the C/N ratio of the bulk soil (Figure 5K) was only a weak predictor of the C/N ratio within the fine <53 µm fraction (R^2 = 0.19, r = 0.44).

In the subsoil, the relationship (Figure 5L) between total SOC and absolute MAOC became exceptionally strong (R^2 = 0.94, r = 0.97). However, unlike the topsoil, the proportion of MAOC in the subsoil showed (Figure 5M) no meaningful dependency on total SOC concentration (R^2 = 0.05, r = −0.22).

Most notably, vertical profile analysis revealed a profound decoupling between surface and subsurface horizons. The absolute SOC concentrations in the topsoil were poor predictors (Figure 5N) of subsoil SOC (R^2 = 0.09, r = 0.30). Furthermore, the structural stabilization mechanisms were completely uncoupled (Figure 5O), as evidenced by the lack of correlation between the MAOC proportions in the topsoil and subsoil (R^2 = 0.01, r = 0.09).

3.8. Soil-Specific Regression Analyses

In the surface horizons (topsoil), the relationship between total SOC and absolute MAOC concentrations was strongly governed by soil types (Figure 6). For Leptosols, a robust positive linear relationship was observed (R^2 = 0.66, r = 0.81, $p < 0.05$). Cryosols also exhibited a significant, albeit more scattered, positive scaling (R^2 = 0.42, r = 0.65, $p < 0.05$). Conversely, in Podzols, the absolute accumulation of SOC showed no significant linear dependency on MAOC (R^2 = 0.23, r = 0.48, p = 0.334).

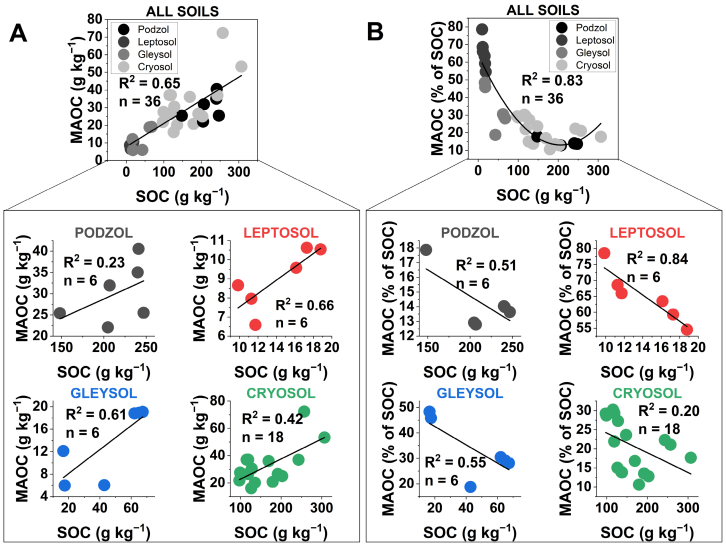


Figure 6. Visualization of soil-specific regression analyses for **topsoil**. (**A**) Relationship between absolute soil organic carbon (SOC, g kg^{-1}) and mineral-associated organic carbon (MAOC, g kg^{-1}) content in four soil types. (**B**) Relationship between absolute SOC (g kg^{-1}) and proportion of MAOC (% of SOC) in four soil types. The exact sample size (n) and R^2 are printed directly on each panel.

In Leptosol topsoil, an increase in total SOC concentration was significantly associated with a decrease in the relative proportion of MAOC (R^2 = 0.84, r = −0.92, $p < 0.05$). In

Podzol topsoils, a similar negative trend was observed, but it did not reach statistical significance at the $\alpha = 0.05$ level ($R^2 = 0.51$, r = −0.71, $p = 0.112$). Interestingly, in Cryosol topsoils, the MAOC proportion remained showed no significant covariance of total SOC concentrations ($R^2 = 0.20$, r = −0.44, $p = 0.065$).

A shift in carbon stabilization paradigms occurred in the subsurface horizons (Figure 7). Here, the relationship between total SOC and absolute MAOC became exceptionally tight and highly significant across all soil types, approaching theoretical maximums of linear dependency. The subsoils of Leptosols ($R^2 = 0.99$, r = 0.99, $p < 0.001$) and Cryosols ($R^2 = 0.97$, r = 0.98, $p < 0.001$) demonstrated near-perfect scaling, while Podzols ($R^2 = 0.89$, r = 0.94, $p = 0.005$) and Gleysols ($R^2 = 0.76$, r = 0.87, $p < 0.05$) also exhibited remarkably strong coupling.

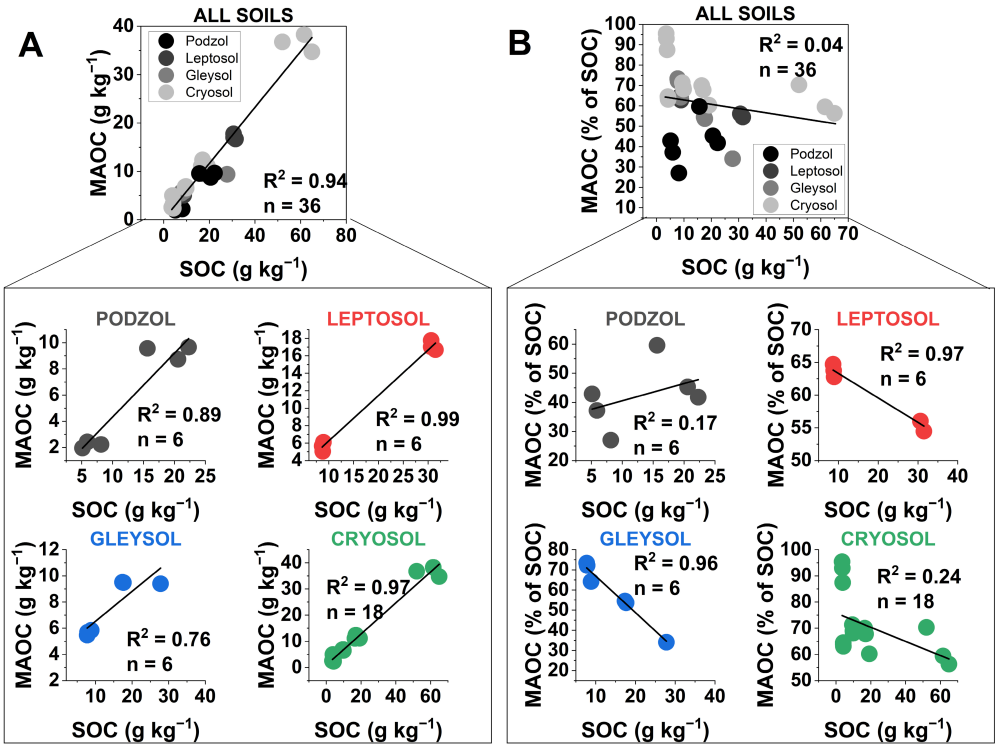


Figure 7. Visualization of soil-specific regression analyses for **subsoil**. (**A**) Relationship between absolute soil organic carbon (SOC, g kg^{-1}) and mineral-associated organic carbon (MAOC, g kg^{-1}) content in four soil types. (**B**) Relationship between absolute SOC (g kg^{-1}) and proportion of MAOC (% of SOC) in four soil types. The exact sample size (*n*) and R^2 are printed directly on each panel.

In the subsoil horizons of Podzols, the proportion of MAOC remained entirely independent of total SOC ($R^2 = 0.17$, r = 0.42, $p = 0.41$). Conversely, the subsoils of Gleysols ($R^2 = 0.97$, r = −0.98, $p < 0.001$) and Leptosols ($R^2 = 0.97$, r = −0.99, $p < 0.001$) exhibited a severe negative relationship, where higher localized carbon accumulations led to a sharp decline in the MAOC proportion. Once again, Cryosols maintained their unique structural rigidity in the subsoil, with the MAOC proportion showing no significant dependency on total SOC ($R^2 = 0.24$, r = −0.49, $p = 0.06$).

It is important to note that with the exception of Cryosols ($n = 18$), each soil type is represented by a limited number of profiles ($n = 6$). While the exceptionally strong subsoil scaling relationships (e.g., $R^2 > 0.97$) are statistically significant, they are based on small group sizes and should therefore be interpreted primarily as descriptive patterns requiring validation with larger sample sets.

4. Discussion

4.1. Pedogenic Controls on Carbon Pool Structure in Surface Horizons

The distribution of SOC pools across the soils of Yamalo-Nenets Autonomous Okrug is governed by the interplay between dominant elementary pedogenic processes (EPPs) and regional climatic constraints. The concept of EPP, originally developed in the Russian pedological tradition [36], conceptualizes soil formation as the superposition of discrete, quasi-independent elementary processes (e.g., podzolization, cryoturbation, gleying, lithogenic accumulation) that operate simultaneously but are driven by distinct environmental controls. In this study, soil taxonomy serves as a proxy for identifying the dominant EPP at each site.

In Podzols, the podzolization process, characterized by intense acid hydrolysis of primary minerals, leaching of base cations, and the illuviation of organo-metallic complexes, creates a highly acidic environment. This severely limits microbial turnover and mineral stabilization capacity [36]. Consequently, Podzol topsoils exhibit a pronounced dominance of particulate organic matter, with POC accounting for approximately 86% of the total SOC pool (Figure 2D). The exceptionally wide bulk C/N ratios (38.5 $\pm$ 5.3) and the persistence of wide C/N ratios within the fine fraction (19.1 $\pm$ 5.7) indicate that stabilization in Podzols is not driven by microbial necromass incorporation [37]. Instead, it results from the downward translocation and sorption of nitrogen-poor, carbon-rich humic and fulvic acids [38]. This acidic illuviation pathway results in a structural decoupling between the massive surface POC accumulation and the underlying mineral matrix, as evidenced by the lack of a significant linear relationship (Figure 6A) between absolute SOC and MAOC concentrations in Podzol topsoils (R^2 = 0.23, p = 0.33).

In stark contrast, Cryosols are shaped by the cryogenic process, where permafrost-induced cryoturbation, frost heaving, and limited biological turnover drive the mechanical incorporation of organic matter into the mineral matrix. The cryogenic EPP generates frozen stabilization paradigm [39,40]. Cryosols accumulate the highest absolute concentration of both SOC (160.7 $\pm$ 59.1 g kg^{-1}) and total nitrogen (10.4 $\pm$ 4.6 g kg^{-1}) in the YNAO, yet the proportional allocation of these elements into stabilized fractions remains remarkably rigid (Figures 2A and 3A). The statistical independence (Figure 6B) of the MAOC proportion from total SOC concentrations in Cryosol topsoils (R^2 = 0.20, p = 0.065) suggests that cryoturbation imposes a structural ceiling on organo-mineral interactions [41]. The proximity to the permafrost table restricts root penetration and microbial activity, effectively conserving organic matter in a state of arrested decomposition rather than active biochemical stabilization [12,42].

Gleysols and Leptosols represent the opposing ends of the pedogenic spectrum in the YNAO. In Gleysols, the gleying process (driven by prolonged waterlogging and anaerobic reduction of Fe and Mn) fosters a bacterial-dominated decomposition pathway [43,44]. This is reflected in the significantly narrower bulk C/N ratios (12.8 $\pm$ 4.9) and the narrowest C/N ratios in fine fraction (10.4 $\pm$ 3.6) among all studied soils, indicating extensive microbial processing and nitrogen enrichment during organo-mineral complexation [45]. The relatively high MAOC (Figure 2C) proportion in Gleysol topsoil (33.4 $\pm$ 11.4%) underscores the efficiency of anaerobic, microbially mediated stabilization. Conversely, Leptosols, governed by the lithogenic (primitive) EPP on shallow, rocky parent materials in the Polar Urals, exhibit the lowest absolute SOC content (Figure 2A) but the highest proportional MAOC dominance (65.1 $\pm$ 8.3%). The thin, undifferentiated profiles of Leptosols facilitate rapid mineral–organic interactions [46], resulting in strong positive scaling between SOC and MAOC (R^2 = 0.99, $p < 0.05$) and extremely narrow C/N ratios (6.9 $\pm$ 2.1), characteristic of highly humified, base-rich organic matter.

4.2. Vertical Stratification and Subsoil Stabilization Mechanisms

While topsoil carbon pools are primarily driven by biogenic inputs and surface-specific EPPs (podzolization, cryoturbation, gleying), the subsoil operates under a regime of strict mineralogical limitation [47]. The strong linear covariance between total SOC and absolute MAOC in the subsoils ($R^2 > 0.97$ in Cryosols and Leptosols) indicates strict scaling between carbon accumulation and mineral sorption. Furthermore, the high measured MAOC proportions (ranging from 42% in Podzols to 71% in Cryosols) demonstrate that mineral association is the quantitatively dominant stabilization pathway in the subsoil, leaving a relatively minor, albeit non-negligible, non-MAOC fraction. This phenomenon suggests that the subsoil mineral matrix acts as a finite sorption sink; once the binding sites are saturated, additional carbon inputs cannot be stabilized and are either leached or remain in a vulnerable, non-protected state [22,27].

Critically, the vertical decoupling of carbon dynamics (Figure 5N) evidenced by the weak relationship between topsoil and subsoil SOC concentrations ($R^2 = 0.09$) and the complete absence of correlation (Figure 5O) between MAOC proportions across depths ($R^2 = 0.01$) demonstrates that surface carbon content cannot be reliably extrapolated to predict deep carbon stabilization [48]. In Podzols, the illuvial translocation of dissolved organic carbon creates a distinct subsurface stabilization zone (Bs/Bh horizons) that operates independently of the overlying organic horizon [49]. In Cryosols, cryoturbation mechanically transports surface-derived organic matter into the permafrost-affected subsoil [50], where it is preserved not by active organo-mineral bonding, but by thermal inhibition of microbial activity [22]. This vertical heterogeneity underscores the necessity of horizon-specific sampling and fractionation in regional carbon inventories, as bulk topsoil measurements systematically misrepresent the true stabilization potential of the deep soil profile.

4.3. Stoichiometric Signatures

The universal narrowing of the C/N ratio upon transition from the bulk pool to the fine fraction across all soil types confirms that microbial necromass and metabolites (characterized by narrow (8–12) C/N ratios) are preferentially stabilized on mineral surfaces [51]. However, the degree of this stoichiometric convergence varies markedly with the dominant EPP. In Podzols, the relatively wide C/N ratio in fine fraction (19) indicates that a significant proportion of the mineral-associated carbon is not microbially derived, but rather represents abiotically sorbed, nitrogen-poor acids translocated from the surface [52]. This non-microbial stabilization pathway is a mark of podzolization and has profound implications for carbon persistence: organo-mineral complexes may be less stable than microbially derived necromass-mineral complexes under changing environmental conditions [53].

In Gleysols and Leptosols, the narrow C/N ratios in fine fraction (10 and 13, respectively) point to a predominantly microbial stabilization pathway, where extensive decomposition and nitrogen cycling precede organo-mineral complexation [53]. The strong negative relationship (Figure 7B) between SOC concentration and MAOC proportion in the subsoils of Gleysols ($R^2 = 0.97$) and Leptosols ($R^2 = 0.96$) further suggests that as carbon inputs increase, the mineral binding sites become saturated [54], leading to a proportional decline in the stabilized fraction. This saturation effect is less pronounced in Cryosols, where cryoturbation continuously renews mineral surfaces and redistributes organic matter, maintaining a more dynamic equilibrium between labile and stabilized pools.

While the relative proportion of MAON did not exhibit stark pairwise differences across all soil taxa, the stoichiometric convergence of the C:N ratio within the fine <53 μm fraction provides critical insights into the nitrogen-driven mechanisms of carbon stabilization. We hypothesize that nitrogen availability acts as a primary bottleneck for microbial processing and subsequent organo-mineral complexation in Arctic soils. In Podzols, the

persistently wide C:N ratios (19 in fine <53 μm fraction) and relatively low MAON content indicate severe nitrogen limitation, which restricts microbial biomass turnover and forces carbon stabilization via abiotic sorption of nitrogen-poor organic acids. Conversely, the narrow C:N ratios (10–13) in fine <53 μm fraction in Gleysols and Leptosols reflect active microbial nitrogen cycling and the preferential stabilization of nitrogen-rich microbial necromass onto mineral surfaces. Thus, even where bulk MAON proportions remain statistically uniform, the C:N stoichiometry reveals that the biochemical quality of stabilized nitrogen fundamentally dictates the pathway and persistence of mineral-associated carbon in the cryopedosphere.

4.4. Chemical Inert Carbon Pool

The iSOC fraction, isolated via aggressive H_2O_2 oxidation, represents the most recalcitrant component of the soil carbon continuum [33,55]. The statistical independence (Figure 5D) of the iSOC proportion from total SOC concentrations across all soil types indicates that the accumulation of this chemically resistant pool is decoupled from contemporary biogenic inputs and is instead governed by long-term pedogenic inertia. The specific origin of the iSOC pool cannot be definitively established from the present dataset. However, based on the existing literature and the regional environmental context, we hypothesize that this oxidation-resistant fraction may comprise a mixture of pyrogenic carbon from historical tundra fires [56], highly condensed aromatic compounds derived from highly degraded, recalcitrant organic residues [57], and deeply humified residues that have persisted through multiple pedogenic cycles. These interpretations remain hypothetical and would require isotopic (^{14}C) or molecular-level validation in future studies.

The relatively high absolute iSOC concentrations in Podzol topsoils (35.4 ± 11.1 g kg^{-1}) may be linked to the preservation of pyrogenic carbon in the acidic, anaerobic microsites of the organic horizon, where oxidative degradation is severely inhibited [57]. In Cryosols, the iSOC pool is likely protected by the physical encapsulation of organic matter within frozen soil aggregates and the chemical stabilization of ancient, highly degraded compounds that are inherently resistant to both biological and chemical oxidation [58]. The identification and quantification of this inert pool are critical for refining regional carbon models, as it represents a chemically resistant baseline fraction whose operational recalcitrance under current and future climatic scenarios is inferred from its operational isolation but not directly demonstrated by the present dataset.

4.5. Implications for Permafrost Carbon Feedback and Limitation of Research

The findings of this study have profound implications for assessing the vulnerability of Arctic soil carbon to climate warming. The pronounced dominance of POC in Podzol and Cryosol topsoils indicates that a substantial fraction of the surface carbon pool is inherently labile and highly susceptible to microbial mineralization upon permafrost thaw or changes in hydrological regime [15]. The wide C/N ratios and acidic conditions in Podzols may temporarily buffer this vulnerability by inhibiting microbial activity; however, any shift toward warmer, drier conditions could rapidly accelerate POC decomposition, releasing significant quantities of CO_2 into the atmosphere [3,6].

Conversely, the near-complete mineral stabilization of subsoil carbon in Cryosols and Leptosols ($R^2 > 0.97$) suggests that deep carbon content is largely protected by mineral sorption capacity rather than by thermal inhibition alone [12,18]. This mineral protection may persist even after permafrost degradation, provided that the soil structure remains intact and anaerobic conditions are maintained [14]. However, in Gleysols, where waterlogging and gleying create reducing conditions, permafrost thaw could lead to the mobilization of

dissolved organic carbon and the transition from CO_2 to CH_4 emissions, fundamentally altering the greenhouse gas balance of the landscape [25].

The vertical decoupling of carbon pools and the taxonomic divergence in stabilization mechanisms underscore the need for soil-type-specific parameterization in regional and global carbon models. Treating the Arctic cryopedosphere as a homogeneous entity, or relying solely on bulk topsoil measurements, will inevitably lead to systematic errors in projecting the magnitude and timing of the permafrost carbon feedback. Future research should prioritize the integration of physical fractionation data, stoichiometric constraints, and horizon-specific stabilization kinetics into regional carbon models to improve the accuracy of climate projections for the rapidly changing Arctic.

It should be acknowledged that the large number of bivariate regression analyses performed across Figures 5–7 increases the probability of type I errors (false-positive findings). While the most robust relationships (e.g., $R^2 > 0.90$ with $p < 0.01$) are unlikely to be spurious, borderline results with p-values near the 0.05 threshold should be interpreted with caution. Future studies with larger sample sizes per soil taxon are needed to confirm the soil-specific regression patterns reported here.

It is important to note that the values reported in this study represent mass concentrations (g kg^{-1}) rather than volumetric stocks (kg m^{-2}). While concentration data provide critical insights into organo-mineral stabilization mechanisms and pedogenic processes, future studies incorporating bulk density and coarse fragment corrections are needed to quantify absolute landscape-scale carbon stocks. This is particularly relevant for highly skeletal soils such as Leptosols, where high stoniness significantly alters the volumetric carbon storage capacity compared to mass-based concentrations.

5. Conclusions

This study demonstrates that the structure of carbon and nitrogen pools in the Russian Arctic cryopedosphere is governed by distinct elementary pedogenic processes—podzolization, cryoturbation, gleying, and lithogenic accumulation—operating under divergent climatic constraints. Topsoil pools are sharply differentiated by soil taxonomy, ranging from POC-dominated Podzols to MAOC-dominated Leptosols, whereas subsoil horizons converge toward strict mineralogical limitation with near-perfect SOC–MAOC scaling. A pronounced vertical decoupling between surface and subsurface stabilization mechanisms renders bulk topsoil measurements inadequate for predicting deep carbon persistence. These findings underscore the necessity of soil-type-specific, horizon-resolved parameterization in regional and global carbon models to accurately project the permafrost carbon feedback under ongoing Arctic warming.

Author Contributions: Conceptualization, T.N. and E.A. (Evgeny Abakumov); methodology, T.N.; software, V.P.; validation, S.Y., X.W. and E.A. (Evgeny Abakumov); formal analysis, A.V., E.A. (Egor Artyukhov), A.S.; investigation, T.N., V.P. and E.A. (Egor Artyukhov); resources, E.A. (Evgeny Abakumov) and S.Y.; data curation, T.N.; writing—original draft preparation, T.N.; writing—review and editing, E.A. (Evgeny Abakumov), S.Y. and X.W.; visualization, A.S.; supervision, X.W.; project administration, X.W. and E.A. (Evgeny Abakumov); funding acquisition, E.A. (Evgeny Abakumov) and X.W. All authors have read and agreed to the published version of the manuscript.

Funding: This research was supported by the Russian Science Foundation (grant No. 24-44-00006) and the National Natural Science Foundation of China (grant No. 32361133551).

Data Availability Statement: The data presented in this study are available on request from the corresponding author. The data are not publicly available due to institutional and national regulations restricting the open dissemination of geospatial and environmental datasets.

Acknowledgments: The authors thank the staff of the Saint Petersburg State University Research Park, particularly the "Chemical Analysis and Materials Research Centre" for analysis of soil samples.

Conflicts of Interest: The authors declare no conflicts of interest.

Appendix A

Table A1. Coordinates of sampling sites for each study area.

Site Name	Podzols Principal Qualifiers Albic/Turbic (*n* = 3), Entic (*n* = 2), Leptic (*n* = 1)	Leptosols Principal Qualifiers Skeletic (*n* = 3), Folic (*n* = 3)	Cryosols Principal Qualifiers Turbic (*n* = 9), Cambic (*n* = 5), Skeletic Histic (*n* = 4)	Gleysols Principal Qualifiers Histic/Folic (*n* = 3), Spodic (*n* = 3)
Lower Ob Basin	66.529265; 66.708518 66.516599; 66.703540 66.503311; 66.709548 66.503667; 66.698333	-	66.469667; 67.500778 66.474883; 67.508592 66.467268; 67.524729 66.691722; 66.194750 66.696405; 66.194868 66.694025; 66.183710 66.688580; 66.300380 66.715000; 66.281389 66.713611; 66.282778	66.506944; 67.037778 66.688110; 66.331854 66.698575; 66.305873 66.696309; 66.234490
Polar Urals	-	66.900278; 65.436667 66.870628; 65.397290 66.871725; 65.394758 66.872315; 65.392783 66.873479; 65.392011 66.871389; 65.403889	66.989667; 65.482972 66.989750; 65.484104 66.866111; 65.411389 66.860833; 65.452778 66.866131; 65.432402	66.868742; 65.407451
Yamal Peninsula	67.860090; 70.501160 67.859780; 71.091050	-	67.856850; 71.088934 67.869953; 71.083398 67.862873; 71.098890 67.870482; 71.112723	67.866533; 71.449008
Total	6	6	18	6

Appendix B

Appendix B.1. Laboratory Analysis and Physical Fractionation

To isolate the MAOC and POC-containing granulometric fractions, a particle-size fractionation procedure was employed following the protocol detailed by Muratore and Welsh [32]. Briefly, a 5 g subsample of the air-dried, 2 mm sieved soil was placed in a conical centrifuge tube and dispersed in 15 mL of 0.5% (*w*/*v*) sodium hexametaphosphate (SHMP) solution. The suspension was agitated on a rotary shaker for 24 h to ensure the complete dispersion of soil microaggregates. The dispersed soil suspension was then carefully poured onto a 53 µm (0.053 mm) sieve and rinsed with an additional 200 mL of 0.5% SHMP solution to guarantee the complete separation of the physical fractions.

The suspension passing through the 53 µm sieve, comprising the silt and clay fraction, was collected, centrifuged at 10,000 rpm for approximately 10 min to recover the fine particles, and subsequently oven-dried at 105 °C. This recovered fraction represents the fine granulometric fraction (<53 µm) with MAOC and MAON. Conversely, the material retained on the 53 µm sieve, comprising the sand and particulate fraction, was collected and dried at 60 °C; this fraction represents the POC. Both the POC fraction (retained on the sieve) and the MAOC/MAON fraction (recovered from the centrifugate) after being oven-dried are weighed directly to assess the procedural mass recovery, which consistently ranged

between 95% and 100%. It is acknowledged that the >53 µm fraction (POC-contained) may contain sand-associated organic carbon in addition to true particulate plant debris.

A methodological caveat should be noted: the POC fraction isolated at 53 µm may include sand-associated organic carbon, particularly in coarse-textured Podzol profiles. While this does not affect the relative comparison of pool structures across soil types, absolute POC concentrations in sandy soils may be slightly overestimated compared to density-separated particulate fractions.

To quantify the inert soil organic carbon (iSOC) fraction, a chemical oxidation procedure using hydrogen peroxide (H_2O_2) was employed to remove the labile and stabilized organic matter fractions [33]. This method isolates the highly recalcitrant, oxidation-resistant carbon pool that persists in soils over long-term persistence. Briefly, a 5 g subsample of the air-dried, 2 mm sieved soil was placed in a heat-resistant glass beaker and treated with 30% (w/w) H_2O_2 solution. The mixture was gently heated on a water bath at approximately 80–90 °C to catalyze the oxidative decomposition of organic compounds. As the vigorous effervescence (release of O_2) subsided, additional aliquots of H_2O_2 were incrementally added to ensure the complete oxidation of the biologically active and humified organic fractions. The oxidation endpoint was determined when the vigorous effervescence completely ceased and the soil matrix retained a stable color. Procedural blanks (reagents without soil) were run concurrently to correct for any background carbon introduced by the reagents. The residual carbon measured after this aggressive oxidation represents the iSOC fraction. It is crucial to note that while POC and MAOC represent physically separated fractions summing to 100% of the recovered mass, iSOC is a chemically isolated parallel assay. Consequently, the iSOC fraction is not mutually exclusive from POC and MAOC but rather represents the highly oxidation-resistant subset of the bulk SOC continuum.

It should be noted that the quantification of the iSOC fraction relied on the Walkley–Black method rather than dry combustion elemental analysis. While suitable for general SOC assessment, wet oxidation may partially underestimate highly condensed, recalcitrant aromatic structures compared to high-temperature combustion. Therefore, the iSOC values reported here should be interpreted as a conservative estimate of the highly oxidation-resistant carbon pool rather than an absolute measure of chemically inert carbon.

Appendix B.2. Statistical Analysis and Data Processing

Following the quantification of carbon and nitrogen in the <53 µm fraction, these absolute concentrations were mathematically recalculated, accounting for the mass proportion of the <53 µm fraction relative to the bulk soil, to estimate the relative structural contributions of mineral-associated organic carbon (MAOC, expressed as % of bulk SOC) and mineral-associated organic nitrogen (MAON, expressed as % of bulk TN). All parameters were calculated using the following equations:

$$\text{MAOC (g kg}^{-1}) = \text{Cf} \times (\text{Mf}/\text{Mb}) \quad \text{(A1)}$$

where Cf is the carbon concentration in the fine (<53 µm) fraction (g kg^{-1}), Mf is the mass of the recovered (<53 µm) fraction (g), and Mb is the mass of the initial bulk soil subsample (5 g).

$$\text{MAON (g kg}^{-1}) = \text{TNf} \times (\text{Mf}/\text{Mb}) \quad \text{(A2)}$$

where TNf is the nitrogen concentration in the fine (<53 µm) fraction (g kg^{-1}), Mf is the mass of the recovered (<53 µm) fraction (g), and Mb is the mass of the initial bulk soil subsample (5 g).

$$\text{MAOC (\% of SOC)} = (\text{MAOC (g kg}^{-1})/\text{SOC (g kg}^{-1})) \times 100 \quad \text{(A3)}$$

$$\text{MAON (\% of TN)} = (\text{MAON (g kg}^{-1})/\text{TN (g kg}^{-1})) \times 100 \quad \text{(A4)}$$

$$\text{POC (\% of SOC)} = 100 - \text{MAOC (\% of SOC)} \quad \text{(A5)}$$

$$\text{iSOC (\% of SOC)} = (\text{iSOC (g kg}^{-1})/\text{SOC (g kg}^{-1})) \times 100 \quad \text{(A6)}$$

where SOC and iSOC are the carbon concentrations (g kg^{-1}) measured in the untreated bulk soil and the H_2O_2 treated residue, respectively.

Descriptive statistics, including mean values and standard deviations (SD), were calculated for all measured soil parameters to characterize the central tendency and dispersion of the carbon and nitrogen pools within each soil type and horizon. Prior to parametric testing, the assumptions of normality and homogeneity of variances were verified using the Shapiro–Wilk and Levene's tests, respectively.

For variables exhibiting severe skewness or heteroscedasticity (e.g., subsoil SOC in Cryosols), data were log-transformed prior to parametric testing, and the robustness of the results was verified using the non-parametric Kruskal–Wallis test.

To evaluate the main effect of soil type (Podzols, Leptosols, Gleysols, and Cryosols) on the absolute concentrations and relative proportions of the carbon and nitrogen fractions, a one-way analysis of variance (ANOVA) was employed. Given that ANOVA only indicates the presence of a global significant difference among the groups, a post hoc Dunn–Sidak test was applied for multiple pairwise comparisons. The Dunn–Šidák correction was selected as it provides appropriate control of the family-wise error rate for the planned pairwise comparisons among four soil groups while maintaining greater statistical power than the more conservative Bonferroni adjustment.

Appendix C

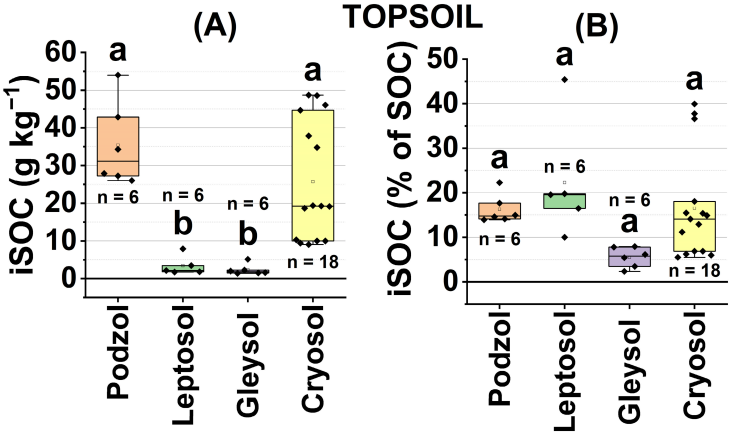


Figure A1. Box plots of measured parameters across soil types in **topsoil** horizons. (**A**) Chemical inert SOC (iSOC) content (g kg^{-1}). (**B**) iSOC proportion (% of SOC). Whiskers indicate standard deviations. The exact sample size (*n*) and post hoc significance (lowercase letters) are printed directly on each panel.

References

1. Miner, K.R.; Turetsky, M.R.; Malina, E.; Bartsch, A.; Tamminen, J.; McGuire, A.D.; Fix, A.; Sweeney, C.; Elder, C.D.; Miller, C.E. Permafrost carbon emissions in a changing Arctic. *Nat. Rev. Earth Environ.* **2022**, *3*, 55–67. [CrossRef]
2. Kögel-Knabner, I.; Amelung, W. Soil organic matter in major pedogenic soil groups. *Geoderma* **2021**, *384*, 114785. [CrossRef]
3. Schuur, E.A.; Abbott, B.W.; Commane, R.; Ernakovich, J.; Euskirchen, E.; Hugelius, G.; Grosse, G.; Jones, M.; Koven, C.; Leshyk, V.; et al. Permafrost and climate change: Carbon cycle feedbacks from the warming Arctic. *Annu. Rev. Environ. Resour.* **2022**, *47*, 343–371. [CrossRef]
4. Pengerud, A.; Dignac, M.F.; Certini, G.; Strand, L.T.; Forte, C.; Rasse, D.P. Soil organic matter molecular composition and state of decomposition in three locations of the European Arctic. *Biogeochemistry* **2017**, *135*, 277–292. [CrossRef]

5. Vonk, J.E.; Tank, S.E.; Mann, P.J.; Spencer, R.G.; Treat, C.C.; Striegl, R.G.; Abbott, B.W.; Wickland, K.P. Biodegradability of dissolved organic carbon in permafrost soils and aquatic systems: A meta-analysis. *Biogeosciences* **2015**, *12*, 6915–6930. [CrossRef]
6. Cui, M.; Ji, D.; Chen, Y. Permafrost response and feedback under temperature stabilization and overshoot scenarios with different global warming levels. *Earth Syst. Dyn.* **2025**, *16*, 1809–1831. [CrossRef]
7. Koven, C.D.; Ringeval, B.; Friedlingstein, P.; Ciais, P.; Cadule, P.; Khvorostyanov, D.; Krinner, G.; Tarnocai, C. Permafrost carbon-climate feedbacks accelerate global warming. *Proc. Natl. Acad. Sci. USA* **2011**, *108*, 14769–14774. [CrossRef]
8. Schuur, E.A.; McGuire, A.D.; Schädel, C.; Grosse, G.; Harden, J.W.; Hayes, D.J.; Hugelius, G.; Koven, C.D.; Kuhry, P.; Lawrence, D.M.; et al. Climate change and the permafrost carbon feedback. *Nature* **2015**, *520*, 171–179. [CrossRef]
9. Wang, J.; Song, C.; Wang, X.; Song, Y. Changes in labile soil organic carbon fractions in wetland ecosystems along a latitudinal gradient in Northeast China. *Catena* **2012**, *96*, 83–89. [CrossRef]
10. Rooney, E.C.; Bailey, V.L.; Patel, K.F.; Possinger, A.R.; Gallo, A.C.; Bergmann, M.; SanClements, M.; Lybrand, R.A. The impact of freeze-thaw history on soil carbon response to experimental freeze-thaw cycles. *J. Geophys. Res. Biogeosci.* **2022**, *127*, e2022JG006889. [CrossRef]
11. Kerketta, N.; Goswami, P.; Roy, A.; Sarma, D.; Farooq, M.; Haider, F.U.; Gogoi, N. Understanding soil carbon durability: Influencing factors, stabilization mechanisms, and research challenges. *Environ. Sustain.* **2026**, *9*, 415–440. [CrossRef]
12. Prater, I.; Zubrzycki, S.; Buegger, F.; Zoor-Füllgraff, L.C.; Angst, G.; Dannenmann, M.; Mueller, C.W. From fibrous plant residues to mineral-associated organic carbon–the fate of organic matter in Arctic permafrost soils. *Biogeosciences* **2020**, *17*, 3367–3383. [CrossRef]
13. Lavallee, J.M.; Soong, J.L.; Cotrufo, M.F. Conceptualizing soil organic matter into particulate and mineral-associated forms to address global change in the 21st century. *Glob. Change Biol.* **2020**, *26*, 261–273. [CrossRef]
14. Hansen, P.M.; Even, R.; King, A.E.; Lavallee, J.; Schipanski, M.; Cotrufo, M.F. Distinct, direct and climate-mediated environmental controls on global particulate and mineral-associated organic carbon storage. *Glob. Change Biol.* **2024**, *30*, e17080. [CrossRef]
15. Sun, S.; Cotrufo, M.F.; Rossel, R.A.V.; Mueller, C.W.; Kida, M.; Hardie, A.G.; Mackay, A.; Krichels, A.H.; Amelung, W.; Kumar, A.; et al. Global hotspots of particulate organic carbon losses under climate change. *Nat. Commun.* **2026**, *17*, 4695. [CrossRef]
16. Kholodov, V.A.; Rogova, O.B.; Lebedeva, M.P.; Varlamov, E.B.; Volkov, D.S.; Ziganshina, A.R.; Yaroslavtseva, N.V. Organic matter and mineral matrix of soils: Modern approaches, definitions of terms and methods of study (review). *Dokuchaev Soil Bull.* **2023**, *117*, 52–100. [CrossRef]
17. Yudina, A.V.; Klyueva, V.V.; Timofeeva, M.V.; Semenov, M.V.; Bardashov, D.R.; Kochneva, M.A.; Mitichkin, D.E.; Fomin, D.S.; Romanenko, K.A. Physical mechanisms of carbon stabilization in soils (a review). *Dokuchaev Soil Bull.* **2025**, *124*, 309–366. (In Russian) [CrossRef]
18. García-Palacios, P.; Bradford, M.A.; Benavente-Ferraces, I.; de Celis, M.; Delgado-Baquerizo, M.; García-Gil, J.C.; Gaitán, J.J.; Goñi-Urtiaga, A.; Mueller, C.W.; Panettieri, M.; et al. Dominance of particulate organic carbon in top mineral soils in cold regions. *Nat. Geosci.* **2024**, *17*, 145–150. [CrossRef]
19. Rovira, P.; Vallejo, V.R. Labile, recalcitrant, and inert organic matter in Mediterranean forest soils. *Soil Biol. Biochem.* **2007**, *39*, 202–215. [CrossRef]
20. Falloon, P.; Smith, P.; Coleman, K.; Marshall, S. How important is inert organic matter for predictive soil carbon modelling using the Rothamsted carbon model? *Soil Biol. Biochem.* **2000**, *32*, 433–436. [CrossRef]
21. Alekseev, I.; Abakumov, E. Soil organic carbon stocks and stability of organic matter in permafrost-affected soils of Yamal region, Russian Arctic. *Geoderma Reg.* **2022**, *28*, e00454. [CrossRef]
22. Nizamutdinov, T.; Bolshiianova, O.; Morgun, E.; Abakumov, E. Molecular composition of humic acids and soil organic matter stabilization rate of the first Arctic carbon measurement supersite "Seven Larches". *Sustainability* **2024**, *16*, 6673. [CrossRef]
23. Wang, W.; Nizamutdinov, T.; Pechkin, A.; Morgun, E.; Li, G.; Wu, X.; Yang, S.; Abakumov, E. Ecological status assessment of permafrost-affected soils in the Nadym Region, Yamalo-Nenets Autonomous District, Russian Arctic. *Land* **2024**, *13*, 1406. [CrossRef]
24. Bartos, A.; Musielok, Ł.; Szymański, W. Stabilization of organic matter in topsoils under different tundra vegetation in central Spitsbergen (High Arctic). *Catena* **2026**, *264*, 109772. [CrossRef]
25. Martens, J.; Mueller, C.W.; Joshi, P.; Rosinger, C.; Maisch, M.; Kappler, A.; Bonkowski, M.; Schwamborn, G.; Schirrmeister, L.; Rethemeyer, J. Stabilization of mineral-associated organic carbon in Pleistocene permafrost. *Nat. Commun.* **2023**, *14*, 2120. [CrossRef]
26. Guo, Y.X.; Yu, G.H.; Hu, S.; Liang, C.; Kappler, A.; Jorgenson, M.T.; Guo, L.; Guggenberger, G. Deciphering the intricate control of minerals on deep soil carbon stability and persistence in Alaskan permafrost. *Glob. Change Biol.* **2024**, *30*, e17552. [CrossRef]
27. Poirier, V.; Basile-Doelsch, I.; Balesdent, J.; Borschneck, D.; Whalen, J.K.; Angers, D.A. Organo-mineral interactions are more important for organic matter retention in subsoil than topsoil. *Soil Syst.* **2020**, *4*, 4. [CrossRef]

28. Artyukhov, E.; Shvetsova, A.; Pokhodnya, E.; Kushnov, I.; Vainberg, A.; Dinkelaker, N.; Nizamutdinov, T.; Abakumov, E. Soil organic matter mineralization rate and metal contamination of the main soil types in central part of Yamal region (West Siberia, Russia). *Carbon Footpr.* **2026**, *5*, 8. [CrossRef]
29. IUSS Working Group WRB. World Reference Base for Soil Resources. In *International Soil Classification System for Naming Soils and Creating Legends for Soil Maps*, 4th ed.; International Union of Soil Sciences: Vienna, Austria, 2022.
30. FAO. *Standard Operating Procedure for Soil pH Determination*; FAO: Rome, Italy, 2021.
31. Yudina, A.; Fomin, D.; Kotelnikova, A.; Milanovskii, E.Y. From the notion of elementary soil particle to the particle-size and microaggregate-size distribution analyses: A review. *Eurasian Soil Sci.* **2018**, *51*, 1326–1347. [CrossRef]
32. Muratore, T.; Welsh, G. Mineral Associated Organic Matter (MAOM) and Particulate Organic Matter (POM) Size Fractionation Protocol. Available online: https://dx.doi.org/10.17504/protocols.io.bp2l6z8o1gqe/v1 (accessed on 28 July 2026).
33. Leifeld, J.; Kögel-Knabner, I. Organic carbon and nitrogen in fine soil fractions after treatment with hydrogen peroxide. *Soil Biol. Biochem.* **2001**, *33*, 2155–2158. [CrossRef]
34. FAO. *Standard Operating Procedure for Soil Organic Carbon: Walkley-Black Method—Titration and Colorimetric Method*; FAO: Rome, Italy, 2019.
35. FAO. *Standard Operating Procedure for Soil Nitrogen—Kjeldahl Method*; FAO: Rome, Italy, 2021.
36. Targulian, V.O.; Krasilnikov, P.V. Soil System and Pedogenic Processes: Self-Organization, Time Scales, and Environmental Significance. *Catena* **2007**, *71*, 373–381. [CrossRef]
37. Zhao, Q.; Bell, S.; Kukkadapu, R.; Richardson, J.; Cliff, J.; Bowden, M.; Leichty, S.; Hofmockel, K.S. Accumulation of soil microbial necromass controlled by microbe–mineral interactions. *Environ. Sci. Technol.* **2025**, *59*, 17558–17570. [CrossRef]
38. Kaiser, K.; Zech, W. Sorption of dissolved organic nitrogen by acid subsoil horizons and individual mineral phases. *Eur. J. Soil Sci.* **2000**, *51*, 403–411. [CrossRef]
39. Startsev, V.V.; Mazur, A.S.; Dymov, A.A. The content and composition of organic matter in soils of the Subpolar Urals. *Eurasian Soil Sci.* **2020**, *53*, 1726–1734. [CrossRef]
40. Beer, C.; Knoblauch, C.; Hoyt, A.M.; Hugelius, G.; Palmtag, J.; Mueller, C.W.; Trumbore, S. Vertical pattern of organic matter decomposability in cryoturbated permafrost-affected soils. *Environ. Res. Lett.* **2022**, *17*, 104023. [CrossRef]
41. Kopittke, P.M.; Dalal, R.C.; Hoeschen, C.; Li, C.; Menzies, N.W.; Mueller, C.W. Soil organic matter is stabilized by organo-mineral associations through two key processes: The role of the carbon to nitrogen ratio. *Geoderma* **2020**, *357*, 113974. [CrossRef]
42. Jansson, J.K.; Tas, N. The microbial ecology of permafrost. *Nat. Rev. Microbiol.* **2014**, *12*, 414. [CrossRef]
43. Zaidelman, F.R. A concept of gleyization and its role in the pedogenesis. *Arch. Agron. Soil Sci.* **1994**, *38*, 323–335. [CrossRef]
44. Bedard-Haughn, A. Gleysolic soils of Canada: Genesis, distribution, and classification. *Can. J. Soil Sci.* **2011**, *91*, 763–779. [CrossRef]
45. Kopittke, P.M.; Hernandez-Soriano, M.C.; Dalal, R.C.; Finn, D.; Menzies, N.W.; Hoeschen, C.; Mueller, C.W. Nitrogen-rich microbial products provide new organo-mineral associations for the stabilization of soil organic matter. *Glob. Change Biol.* **2018**, *24*, 1762–1770. [CrossRef]
46. Bimüller, C.; Naumann, P.S.; Buegger, F.; Dannenmann, M.; Zeller, B.; von Lützow, M.; Kögel-Knabner, I. Rapid transfer of 15N from labeled beech leaf litter to functional soil organic matter fractions in a Rendzic Leptosol. *Soil Biol. Biochem.* **2013**, *58*, 323–331. [CrossRef]
47. Purwaningsih, R.; Hartanti, H.; Hatta, D.A.; Ariyanti, S.D.; Putri, H.A.; Paradisa, D.A.; Dewi, I.K.; Priyawati, E.G.; Stakhis, E.P.; Salsabila, G.; et al. Subsoil mineralogy as environmental factors in controlling topsoil material in the Menoreh-Sumbing volcanic structural transitional landscape, Central Java. *J. Water Land Dev.* **2025**, *67*, 73–85. [CrossRef]
48. James, J.; Devine, W.; Harrison, R.; Terry, T. Deep soil carbon: Quantification and modeling in subsurface layers. *Soil Sci. Soc. Am. J.* **2014**, *78*, S1–S10. [CrossRef]
49. Jansen, B.; Nierop, K.G.; Verstraten, J.M. Mechanisms controlling the mobility of dissolved organic matter, aluminium and iron in podzol B horizons. *Eur. J. Soil Sci.* **2005**, *56*, 537–550. [CrossRef]
50. Lupachev, A.; Abakumov, E.; Gubin, S. The influence of cryogenic mass exchange on the composition and stabilization rate of soil organic matter in cryosols of the Kolyma Lowland (North Yakutia, Russia). *Geosciences* **2017**, *7*, 24. [CrossRef]
51. Wang, X.; Kallenbach, C.M.; Almaraz, M.; Georgiou, K.; Sun, L.; Sang, C.; Jiang, P.; Liu, Y.; Bai, E.; Wang, C. Clay-organic matter interactions drive microbial necromass preservation in soils. *Nat. Commun.* **2026**, *17*, 3368. [CrossRef]
52. Mikutta, R.; Turner, S.; Schippers, A.; Gentsch, N.; Meyer-Stüve, S.; Condron, L.M.; Peltzer, D.A.; Richardson, S.J.; Eger, A.; Hempel, G.; et al. Microbial and abiotic controls on mineral-associated organic matter in soil profiles along an ecosystem gradient. *Sci. Rep.* **2019**, *9*, 10294. [CrossRef]
53. Hu, P.; Zhang, W.; Nottingham, A.T.; Xiao, D.; Kuzyakov, Y.; Xu, L.; Chen, H.; Xiao, J.; Duan, P.; Tang, T.; et al. Lithological controls on soil aggregates and minerals regulate microbial carbon use efficiency and necromass stability. *Environ. Sci. Technol.* **2024**, *58*, 21186–21199. [CrossRef]

54. Hassink, J. The capacity of soils to preserve organic C and N by their association with clay and silt particles. *Plant Soil* **1997**, *191*, 77–87. [CrossRef]
55. Semenov, V.M.; Lebedeva, T.N.; Semenov, M.V.; Sokolov, D.A.; Zinyakova, N.B.; Udal'tsov, S.N. Structural, process-related and functional pools of organic matter in different soil types and land uses of the European territory of Russia. *Agric. Chem.* **2025**, *11*, 3–16. [CrossRef]
56. Abakumov, E.; Pechkin, A.; Chebykina, E.; Shamilishvili, G. Effect of the wildfires on sandy podzol soils of Nadym region, Yamalo-Nenets Autonomous District, Russia. *Appl. Environ. Soil Sci.* **2020**, *2020*, 8846005. [CrossRef]
57. Andrey, Y.; Moskovchenko, D.; Sedov, S.; Sharapov, D.; Shvartseva, O. The impact of fires on the fractional composition of iron and carbon dynamics in the cryogenic soils of the forest–tundra of Western Siberia under changing climate conditions. *Soil Syst.* **2025**, *9*, 15. [CrossRef]
58. Diochon, A.; Gregorich, E.G.; Tarnocai, C. Evaluating the quantity and biodegradability of soil organic matter in some Canadian Turbic Cryosols. *Geoderma* **2013**, *202*, 82–87. [CrossRef]

Disclaimer/Publisher's Note: The statements, opinions and data contained in all publications are solely those of the individual author(s) and contributor(s) and not of MDPI and/or the editor(s). MDPI and/or the editor(s) disclaim responsibility for any injury to people or property resulting from any ideas, methods, instructions or products referred to in the content.